Environmental Science Nano

Mobility of Soil-Biodegradable Nanoplastics in Unsaturated Porous Media Affected by Protein-Corona

Journal:	*Environmental Science: Nano*
Manuscript ID	EN-ART-02-2024-000140.R1
Article Type:	Paper

Environmental Science Nano

PAPER

Cite this: DOI: 00.0000/xxxxxxxxxx

Mobility of Soil-Biodegradable Nanoplastics in Unsaturated Porous Media Affected by Protein-Corona†

Yingxue Yu[a], Odeta Qafoku[b], Libor Kovarik[b], Anton F. Astner[c], Douglas G. Hayes[c], Markus Flury*[d,e]

Received Date
Accepted Date

DOI: 00.0000/xxxxxxxxxx

Soil-biodegradable plastic has been increasingly used as mulches in agriculture, which provides not only agronomical benefits but also in-situ disposal and biodegradation options. However, soil-biodegradable plastic mulches inevitably fragment into micro- and nanoplastics during biodegradation, which can reside in soils or migrate into deep soils, where they may not degrade readily due to reduced microbial activity. To date, little is known about the transport of soil-biodegradable micro- and nanoplastics in soils. Here, we studied the transport of soil-biodegradable nanoplastics (∼200 nm) made of polybutylene adipate co-terephthalate (PBAT) in unsaturated sand (proxy for soil). Specifically, we studied the mobility of pristine and weathered PBAT nanoplastics in the absence and presence of proteins (positively charged lysozyme and negatively charged bovine serum albumin, pH = 7.7). We found that (1) both pristine and the weathered PBAT nanoplastics were mobile; (2) positively charged lysozyme formed protein-coronas around PBAT nanoplastics and inhibited the transport; and (3) decreased water saturation promoted the retention of PBAT nanoplastics via physical straining. These results suggest that soil-biodegradable nanoplastics fragmented from soil-biodegradable plastic mulches are mobile and may readily migrate into deep soil layers, but positively charged proteins and unsaturated flow would prevent such transport via formation of protein-corona and physical straining.

Environmental significance

Soil-biodegradable plastic mulch degrades in situ, serving as a promising alternative to conventional polyethylene mulch and alleviating agriculture plastic pollution. During breakdown, soil-biodegradable plastic mulch forms micro- and nanoplastics, which can migrate into deeper soil layers, where slower microbial activities could hinder the biodegradation of these micro- and nanoplastics. Our findings suggest that soil-biodegradable nanoplastics (∼200 nm) are highly mobile, but protein corona formation with positively charged proteins and unsaturated flow can hinder their transport. Therefore, soil-biodegradable micro- and nanoplastics are likely to remain in the topsoil, where complete biodegradation would occur to ensure long-term sustainability of the soil-biodegradable plastic mulch.

1 Introduction

Plastic pollution has become an environmental threat, affecting not only aquatic but also terrestrial ecosystems. Recently, agricultural soils have been identified as a unique hotspot of plastic pollution, receiving plastics from multiple agricultural practices, including biosolids application, compost amendments, waste water irrigation, and plastic mulching[1–3]. Plastic pollution of agricultural soils may impair soil function or impede plant growth, threatening food safety and security[4,5]. Thus, solutions are urgently needed to reduce the input of plastics into agricultural soils from these agricultural practices while maintaining their benefits. Under such a scope, increasing attention has been paid to soil-

[a] Department of Environmental Science & Forestry, The Connecticut Agricultural Experiment Station, New Haven, CT 06511, USA.
[b] Pacific Northwest National Laboratory, Richland, WA 99354, USA.
[c] Department of Biosystems Engineering & Soil Science, The University of Tennessee, Knoxville, TN, 37996, USA.
[d] Department of Crop & Soil Sciences, Puyallup Research & Extension Center, Washington State University, Puyallup, WA 98371, USA.
[e] Department of Crop & Soil Sciences, Washington State University, Pullman, WA 99164, USA.

† Electronic Supplementary Information (ESI) available: Details on preparations of nanoplastics, DLVO calculations, transport experiments, hydrodynamic diameters, Figures on water potentials, DLVO profiles, plastic breakthrough curves, UV-vis spectra, and calibration curves. See DOI: 00.0000/00000000.

biodegradable plastic mulches, which provide not only satisfying agronomical performance but also in-situ disposal and biodegradation options, and thus are regarded as an eco-friendly alternative to conventional plastic mulches[6].

Soil-biodegradable plastic mulches are designed to be intentionally incorporated into soils after the growing season. Upon application and soil-incorporation, soil-biodegradable plastic mulches gradually fragment into macro-, micro-, and nanoplastics (plastic particles with size $>$ 5 mm, 100 nm–5 mm, and $<$ 100 nm, respectively[7,8]), and are metabolized by soil microorganisms and converted into CO_2, H_2O, and microbial biomass[9,10]. This soil-biodegradable feature implies that soil-biodegradable plastic mulches, unlike conventional plastic mulches, do not produce persistent micro- and nanoplastics in soils. However, the biodegradation does not occur instantaneously, but instead, may take several years depending on the properties of soil-biodegradable plastic mulches as well as the environmental conditions[11–13]. Therefore, it is inevitable for soil-biodegradable plastic mulches to generate soil-biodegradable micro- and nanoplastics that temporarily reside in soils[8].

Studies have shown that soil-biodegradable micro- and nanoplastics may cause similar negative impacts to soil ecosystems as conventional micro- and nanoplastics. For example, Schopfer et al.[14] observed a decrease in the number of offspring and body length of a soil-dwelling nematode (*Caenorhabditis elegans*) when they were exposed to suspensions that contained 1, 10, or 100 mg/L of either polyethylene microplastics or biodegradable microplastics made of polylactic acid (PLA) and polybutylene adipate co-terephthalate (PBAT) on agar plates; but the results were not consistent among all treatments. Qi et al.[15] found that both soil-biodegradable (PBAT) and low-density polyethylene microplastics increased saturated hydraulic conductivity and field capacity while decreased bulk density of a sandy soil at concentrations $>$1% w/w. However, the applicability of these studies is yet to be validated, because little is known about the amount of soil-biodegradable plastic introduced into the environment as well as the fate and transport of soil-biodegradable micro- and nanoplastics in the environment.

To fill this knowledge gap, we studied the effects of UV-weathering and protein-corona on the transport of soil-biodegradable nanoplastics under unsaturated flow conditions. We selected a soil-biodegradable plastic mulch made of PBAT to generate soil-biodegradable nanoplastics, considering that PBAT is the most commonly used synthetic polymer in soil-biodegradable plastic mulch, owing to its biodegradability in soils and similarity in physical properties to linear low-density polyethylene. UV-weathering and formation of protein-corona are common environmental modifications that occur to soil-biodegradable plastics during biodegradation, and these modifications have been shown to significantly change surface properties, stability, and mobility of conventional and soil-biodegradable nanoplastics[16–18]. The effect of UV-weathering was studied with pristine and weathered soil-biodegradable nanoplastics and the effect of protein-corona was studied with positively charged proteins, i.e., lysozyme, as well as negatively charged proteins, i.e., bovine serum albumin. We also compared the transport of the soil-biodegradable nanoplastics with that of commercially available polystyrene nanospheres, as polystyrene nanospheres have been studied intensively in the literature to elucidate the mechanisms controlling fate and transport of nanoplastics in the environments[16,17,19]. We hypothesized that (1) UV-weathering enhances the transport of soil-biodegradable nanoplastics because the plastic surface becomes more negatively charged; (2) the positively charged lysozyme hinders the transport; and (3) the negatively charged bovine serum albumin promotes the transport.

2 Materials and Methods

2.1 Nanoplastics and proteins

Pristine soil-biodegradable nanoplastics with mean particle size of $\sim$200 nm were prepared via fragmentation and filtration from a black soil-biodegradable plastic mulch film made with PBAT (BioAgri, BioBag Americas, Dunedin, FL). Weathered PBAT nanoplastics with mean particle size of $\sim$200 nm were prepared by exposing pristine soil-biodegradable particles to 840 h of radiation in an Atlas SunTest CPS+ solar simulator equipped with a 1 kW Xenon Arc Lamp (wavelength: 300–800 nm, 650 W/m^2) (Atlas Material Testing Technology LLC, Mount Prospect, IL). Stock solutions of pristine and weathered soil-biodegradable nanoplastics were obtained at concentrations of 200 mg L^{-1} and 180 mg L^{-1}, respectively. Details about the preparation methods are given in the Supporting Information, Section S1.

Carboxylate-modified polystyrene (PS-COOH) nanospheres (220 nm in diameter, PC02N, Lot Nr. 6481, Bangs Laboratories, Inc., Fishers, IN) were purchased to prepare the stock solution of PS-COOH nanoplastics (500 mg L^{-1}). The PS-COOH nanospheres were used as reference material against which the transport of the PBAT nanoplastics were compared, as PS-COOH nanospheres have been commonly used as model nanoplastics to study the fate and transport in the literature[16,17,19].

Protein stock solutions of 1000 mg L^{-1} were prepared from positively charged lysozyme (LSZ, molecular weight is 14.3 kDa, isoelectric point is pH 11, L6876, MilliporeSigma, Burlington, MA) and negatively charged bovine serum albumin (BSA, molecular weight is 66.5 kDa, isoelectric point is pH 4.7, A8806, MilliporeSigma, Burlington, MA). All stock solutions were freshly prepared with deionized water and kept at 4 ^{o}C before the transport experiments.

2.2 Characterization of nanoplastics

We determined the weathering effect on PBAT particles with Attenuated Total Reflectance Fourier-transformed Infrared Spectroscopy (ATR-FTIR, IRAffinity-1, Shimadzu Co., Tokyo, Japan; MIRacle ATR, PIKE Technologies, Madison, WI) and collected FTIR spectra of pristine and weathered PBAT particles. To characterize the interaction between nanoplastics and proteins, we first conducted aggregation and sedimentation tests right after suspending pristine PBAT nanoplastics, or weathered PBAT nanoplastics, or PS-COOH nanoplastics (each at 50 mg L^{-1}) in a background solution (0.4 mM $NaHCO_3$ and 9.6 mM NaCl, pH = 7.7 $\pm$ 0.5) in the absence or presence of proteins (10 mg L^{-1} of LSZ or BSA). The background solution was chosen to provide

a controlled ionic strength and pH.

Dynamic light scattering (DLS) measurements were conducted with a Zetasizer Nano ZS (Malvern Instruments Ltd., Malvern, UK) to obtain aggregation profiles of PBAT and PS-COOH nanoplastics for 60 min. Electrophoretic mobility of the nanoplastics was measured at the end of DLS measurements on the same sample with the Zetasizer and converted to ζ-potentials with the Smoluchowski equation. Contact angles were determined with the sessile drop method with different liquids and with a goniometer (Drop Shape Analysis System, DSA100, Krüss GmbH, Hamburg, Germany) following the protocol described in Shang et al.[20] (see Supporting Information Section S2 for more details).

Sedimentation of the three nanoplastics was examined by measuring the absorbance of the nanoplastic suspensions with UV-vis spectrometry (wavelength of 240 nm for pristine and weathered PBAT nanoplastics and 260 nm for PS-COOH nanoplastics, UV-Vis spectra and concentration calibration curves are shown in Figures S1,S2). Nanoplastics suspensions (50 mg/L, 3 mL) with and without proteins were pipetted into a quartz cuvette with 10 mm path length, which was then inserted into the spectrometer and the absorbance was measured at 5-min intervals for 60 min.

The nanoplastics, with and without protein-corona formed after 60 min contact time, were imaged with transmission electron microscopy (FEI Titan 80–300 kV Environmental Transmission Electron Microscope, ETEM, FEI Company). Suspensions were prepared by mixing the stock solutions to the appropriate concentrations as described above. A drop of the nanoplastic suspension was then taken with a pipette and drop-casted onto a TEM copper grid containing a Lacey carbon film and continuous layer of ultrathin carbon film. A Kimtech paper wipe was used to wick the suspension through the Lacey carbon and deposit the nanoplastics on the carbon. The TEM grid was subsequently placed into a TEM holder and inserted into the vacuum of TEM. The observations were carried out at 300 kV, in a conventional TEM mode. The image acquisition was performed with a CCD camera (Gatan UltraScan1000 2k $\times$ 2k) in Gatan Digital Micrograph.

2.3 Column setup

The transport experiments were carried out with the same unsaturated flow system used in our previous studies[21,22]. Briefly, the system consisted of a Plexiglass column (5-cm inner diameter and 15-cm length), a perforated bottom metal plate covered with a 20 μm nylon membrane (NM-E #635, Gilson Company, Inc., Lewis Center, OH), and a hanging water tube connected at the bottom of the metal plate to provide suction and establish unsaturated flow in the column. Inflow was injected with a peristaltic pump and a 12-needle sprinkler at the top of the column, and outflow was sampled with a fraction collector. The Plexiglass column was dry-packed with silica sand (grain size: 250–425 μm, washed with 2 M HCl and deionized water, 3382-05, Mallinckrodt Baker, Inc., Phillipsburg, NJ) in 1-cm increments. The packing resulted in a bulk density of 1.70 g cm^{-3} and porosity of 0.36 cm^3 cm^{-3}. Two tensiometers were installed on the side of the column at 4 cm and 11 cm from the top to monitor the matric potential, which was recorded with pressure transducers connected to a datalogger (CR23X, Campbell Scientific Inc., Logan, UT).

2.4 Transport experiments

Once the unsaturated flow system was set up, deionized water was introduced until a steady unsaturated flow condition (effective saturation: $S = \sim$45 or 85%) was established, i.e., when the two tensiometers show the same readings (representative tensiometers readings are illustrated in Figure S3). Then, a tracer experiment was conducted by injecting 0.2 mM $NaNO_3$ for $\sim$1 pore volume followed with deionized water for $\sim$4 pore volumes. By analyzing $NaNO_3$ concentration in the outflow with UV-vis spectrophotometry at 220 nm, we obtained tracer breakthrough curves, which were then fitted with the standard convection-dispersion equation in Hydrus-1D[23] to calculate the dispersion coefficient (D). After the tracer experiment, the column was flushed with 3 pore volumes of the background solution, and followed with the transport experiment of PBAT nanoplastics (experimental conditions, including flow rates and water contents are summarized in Table S1, Supporting Information).

For the transport experiment, we introduced nanoplastics (pristine PBAT or weathered PBAT or PS-COOH, 50 mg L^{-1}) in the absence or presence of proteins (LSZ or BSA, 10 mg L^{-1}) suspended in the background solution into the column. All inflow suspensions of nanoplastics were freshly prepared from the stock solutions and sonicated for 10 min right before the transport experiment. After $\sim$1 pore volume, the column was flushed with the background solution for 4 pore volumes. Concentrations of nanoplastics in the outflow were measured with UV-vis spectrophotometry at a wavelength of 240 nm for PBAT nanoplastics and 260 nm for PS-COOH nanoplastics (3 mL in a quartz cuvette with 10 mm path length), and neither the positively charged LSZ nor the negatively charged BSA interfered with the absorbance of nanoplastics (absorbance of LSZ and BSA at 240 and 260 nm was 0, see the spectra in Figure S4). Breakthrough curves of nanoplastics were plotted as normalized effluent concentrations (C/C_0, where C is the effluent concentration, C_0 is the initial concentration) as a function of pore volume.

2.5 Interaction energy calculations

We calculated the total interaction energy between nanoplastic particles and between nanoplastics and collector surfaces (i.e., sand-water interfaces and air-water interfaces) with the classical Derjaguin-Landau-Verwey-Overbeek (DLVO) theory and the extended DLVO theory that included the Lewis acid-base interaction energy. In addition, we calculated the total interaction energy with the modified DLVO theory to consider the steric interaction exerted by the formation of protein-corona. Details of the interaction energy calculations are given in the Supporting Information, Section S2.

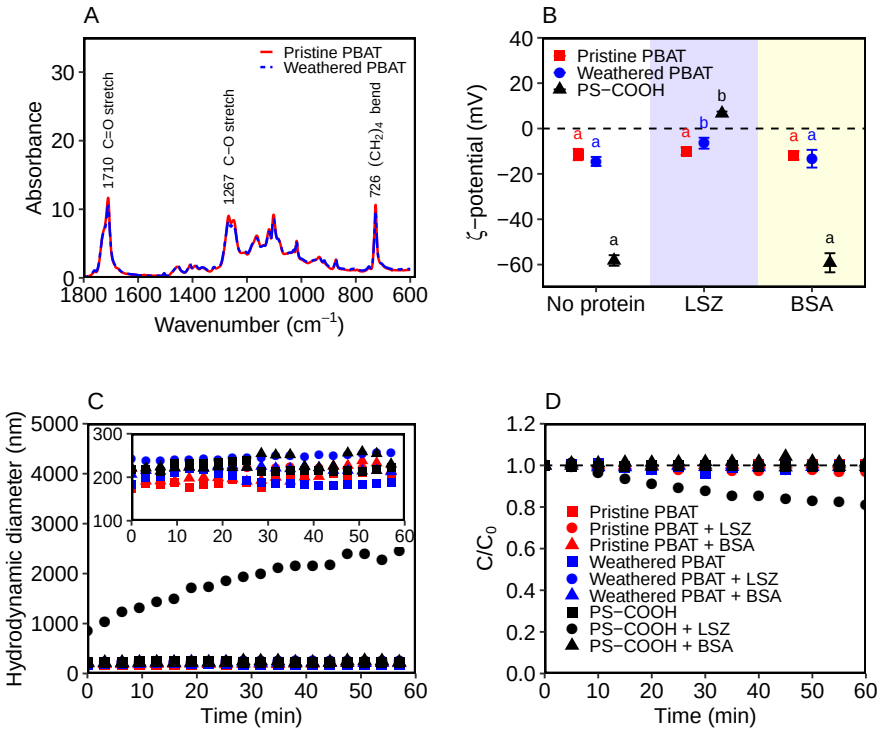

Fig. 1 Physicochemical and colloidal properties of nanoplastics. (A) FTIR spectra of pristine and weathered PBAT particles; (B) ζ-potentials, (C) aggregation profiles, and (D) sedimentation curves of pristine PBAT nanoplastics, weathered PBAT nanoplastics, and PS-COOH nanospheres in the absence and presence of LSZ or BSA (10 mg L^{-1}). FTIR spectra show the average of nine measurements, and characteristic peaks are assigned according to Hayes et at. (2017)[24]. ζ-potentials show mean $\pm$ standard deviation of nine measurements, and different letters indicate significant differences between no protein, LSZ, and BSA for one type of nanoplastics (Tukey's Multiple Comparison, $p = 0.01$). Aggregation profiles and sedimentation curves are averages of four measurements, and insert shows a magnification of the y-axis in the aggregation profiles. ζ-potentials, aggregation profiles, and sedimentation curves were determined in the background solution consisting of 0.4 mM $NaHCO_3$ and 9.6 mM NaCl (pH $= 7.7 \pm 0.5$). PBAT: polybutylene adipate co-terephthalate; PS-COOH: carboxylate-modified polystyrene; LSZ: lysozyme; BSA: bovine serum albumin.

3 Results and Discussion

3.1 Physicochemical and colloidal properties of nanoplastics

3.1.1 UV-weathering changes surface properties of PBAT nanoplastics

FTIR analysis revealed that the solar radiation induced weathering of the PBAT particles (Figure 1A). Compared to the pristine PBAT particles, the weathered PBAT particles had a lower relative intensity of characteristic peaks at 1710 cm^{-1} (C=O stretch), 1267 cm^{-1} (C-O stretch), and 726 cm^{-1} ($(CH_2)_4$ bend). In addition, the carbonyl index, which is the ratio of the carbonyl peak (C=O) at 1710 cm^{-1} to the reference methylene peak (CH_2) at 1452 cm^{-1}, decreased from 7.3 to 5.9 after the solar radiation, indicating that the weathered PBAT particles had undergone photolysis and/or hydrolysis[25,26]. Additionally, the weathering effect is demonstrated by the more negative ζ-potential of weathered PBAT nanoplastics in the absence of proteins (-14.5 ± 2.0 mV, mean $\pm$ standard deviation, $n = 9$) relative to that of the pristine PBAT nanoplastics (-11.5 ± 2.5 mV) (Figure 1B). Further, the weathering decreased the water contact angle of PBAT particles from 70 ± 3^o to 61 ± 3^o (mean $\pm$ standard deviation, $n = 12$). These results agree well with previous studies where UV-weathering has been found to introduce more O-containing functional groups, thus increasing the negative charge and decreasing the hydrophobicity of nanoplastics[16,18].

Despite the different ζ-potential and hydrophobicity, both pristine and weathered PBAT nanoplastics did not aggregate and remained stable in the background solution (Figure 1C,D), indicating an overall repulsive interaction between nanoplastics. Indeed, the interaction energies were calculated to be repulsive between PBAT nanoplastics with the classical DLVO theory, with the energy barriers being 2.9 kT and 5.7 kT for pristine and weathered PBAT, respectively (Figure S5A). Although relatively low, the energy barriers would be higher if surface roughness and non-spherical geometry of nanoplastics were considered in the classical DLVO calculations, thus becoming sufficient for the stability of PBAT nanoplastics[27–29]. However, the total interaction energies became less repulsive for pristine and weathered PBAT (-0.007 and 0.09 kT, respectively), when the hydrophobic interaction was included in the form of Lewis acid-base free energy of adhesion (Figure S5B). This suggests that considering hydrophobic interaction leads to underestimation of the high stability of pristine and weathered PBAT nanoplastics; thus, we did not include the hydrophobic interaction between nanoplastics in further DLVO calculations.

3.1.2 Interactions between nanoplastics and proteins

The pristine PBAT, weathered PBAT, and PS-COOH nanoplastics interacted differently with the positively charged LSZ and the negatively charged BSA. As shown in Figure 1B, the ζ-potential of pristine PBAT nanoplastics was not significantly affected by the presence of proteins (ζ-potentials $= -10.0 \pm 1.6$ mV and -11.9 ± 1.8 mV, $p = 0.28$ and $p = 0.88$ in the presence of LSZ and BSA, respectively). However, the ζ-potential of weathered PBAT nanoplastics increased in the presence of LSZ (-6.5 ± 2.4 mV, $p < 0.01$), but remained unchanged in the presence of BSA (-13.3 ± 3.9 mV, $p = 0.66$). Compared with the pristine and weathered PBAT nanoplastics, the PS-COOH nanospheres had a substantially lower ζ-potential (-58.2 ± 2.3 mV), which can be attributed to the carboxylate functionalization of the nanospheres. Similar to the weathered PBAT nanoplastics, the PS-COOH nanospheres showed an increase in ζ-potential in the presence of LSZ, and even a charge reversal was observed (6.7 ± 0.8 mV, $p < 0.001$). These results suggest that the positively charged LSZ increases ζ-potentials of the nanoplastics, especially when the nanoplastics are more negatively charged, while the negatively charged BSA did not affect ζ-potentials of the nanoplastics.

The aggregation tests further corroborated the different interactions of the three nanoplastics with LSZ and BSA. The aggregation profiles show that the hydrodynamic diameter of the pristine and weathered PBAT nanoplastics remained constant in the background solution in the presence of LSZ and BSA (Figure 1C). Although not inducing aggregation, LSZ and BSA increased the hydrodynamic diameters of pristine and weathered PBAT nanoplastics by about 20 nm, except for LSZ and weathered PBAT, where the diameter increased by about 50 nm (Table S2). Similarly, the PS-COOH nanospheres did not aggregate in the presence of BSA, but BSA increased the hydrodynamic diameter of the PS-COOH nanospheres from 222 to 230 nm (Table S2). However, in contrast to the pristine and weathered PBAT nanoplastics, the PS-COOH nanospheres aggregated in the presence of LSZ, as indicated by the increasing hydrodynamic diameter over time, reaching 2,200 nm after 60 min. Consistent with the aggregation results, the sedimentation tests showed that the pristine and weathered PBAT nanoplastics remained stable in the presence of proteins, and only the PS-COOH aggregated and settled out in the presence of LSZ (Figure 1D).

The observed increase in hydrodynamic diameters is likely due to the formation of a protein-corona around the nanoplastics, as reported for polystyrene nanospheres in previous studies[17,19,30]. TEM imaging revealed that in the absence of proteins, both pristine and weathered PBAT nanoplastics had oblong or round shape with irregular edges (Figure 2A,B), while standard PS-COOH nanoplastics were perfectly spherical (Figure 2C). The intrinsic sizes of the three nanoplastics matched their hydrodynamic diameters (197 ± 12 nm for pristine PBAT, 196 ± 11 nm weathered PBAT, and 222 ± 7 nm for PS-COOH nanoplastics, mean $\pm$ standard deviation, $n = 4$). Both LSZ and BSA were found to attach onto the surfaces of nanoplastics, and formed a protein-corona (Figure 2D,E,F). Besides, the positively charged LSZ seemed to form a more complete protein-corona around nanoplastics than the negatively charged BSA (Figure 2D,E), which is likely due to the attractive electrostatic forces between positively charged LSZ and negatively charged nanoplastics[19,31].

Previous studies have shown that protein-coronas can introduce steric repulsive interactions between colloidal particles and thus stabilize colloidal particles, including nanoplastics[32–34]. Indeed, when the steric force was included in the DLVO calculation, the total interaction energy became more repulsive and even an infinite energy barrier developed between nanoplastics (Figure S6). However, in the presence of BSA, the classical DLVO theory already predicted a high stability of pristine PBAT, weathered PBAT, and PS-COOH nanoplastics, suggesting a primary role of the electrostatic force while a secondary role of the steric force in particle-particle interaction.

Further, the repulsive steric interaction contradicted our observation that PS-COOH nanospheres aggregated in the presence of LSZ. This indicates that other mechanisms, for instance, electrostatic interaction and the attractive patch-charge interaction, were responsible for the aggregation of PS-COOH nanospheres[17]. A similar finding was reported by Dong et al.[19], who found that polystyrene nanospheres (200 nm) aggregated substantially in the presence of LSZ. They attributed the aggregation to the attractive patch-charge interaction, where the incomplete and uneven coverage of LSZ on nanospheres led LSZ-rich areas of nanospheres to complex with LSZ-poor areas of other nanospheres. However, the attractive patch-charge interaction can not explain the stability of the pristine and weathered PBAT nanoplastics in the presence of LSZ, which is likely due to the limited charge modification induced by LSZ for PBAT nanoplastics. Overall, these results suggest that although LSZ and BSA formed protein-coronas around nanoplastics, the protein-coronas did not exert sufficient steric forces to enhance the stability of nanoplastics, but rather could hinder electrostatic repulsion.

3.2 Transport of nanoplastics

3.2.1 Unsaturated flow conditions and breakthrough curves

Figures S7 shows representative tracer breakthrough curves under two saturations. The mass recovery of all tracer breakthrough curves were around 100%, indicating that there was no immobile water in the column. Besides, the tracer breakthrough curves were well fitted with the standard convection-dispersion equation ($R^2 > 0.98$), meaning that the unsaturated flow conditions were steady and uniform during the experiments. Further, the fitted dispersion coefficients under the lower water saturation ($D = 0.98 \pm 0.09$ cm^2 min^{-1}, $n = 12$, $S = \sim$45%) were larger than that under the higher water saturation ($D = 0.12 \pm 0.03$ cm^2 min^{-1}, $n = 12$, $S = \sim$85%), suggesting a more important role of dispersion under low water saturation[35].

Figure 3 shows the breakthrough curves of nanoplastics at two saturations in the absence or presence of proteins. The pristine PBAT, weathered PBAT, and PS-COOH nanoplastics arrived at similar times in the effluents as the tracer, indicating that size exclusion did not occur during the transport[36,37]. The pristine and weathered PBAT nanoplastics were mobile under all experimental conditions, with the recovery in the effluent (M_{eff}) ranging

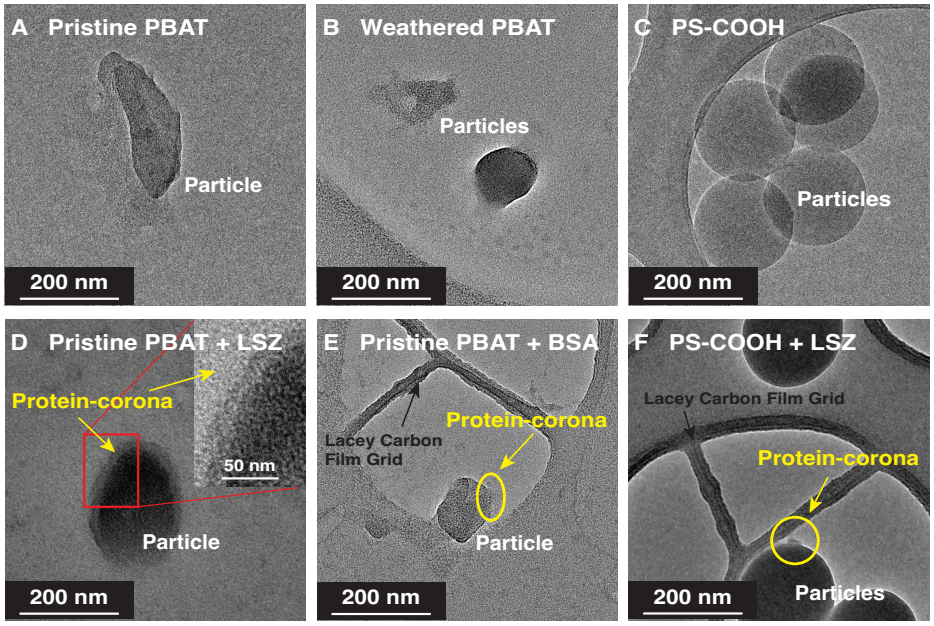

Fig. 2 TEM images of nanoplastics in the absence and presence of proteins. (A) Pristine PBAT nanoplastics in the background solution; (B) Weathered PBAT nanoplastics in the background solution; (C) PS-COOH nanoplastics in the background solution; (D) Pristine PBAT nanoplastics with LSZ in the background solution; (E) Pristine PBAT nanoplastics with BSA in the background solution; (F) PS-COOH nanoplastics with LSZ in the background solution. The background solution consisted of 0.4 mM $NaHCO_3$ and 9.6 mM NaCl (pH = 7.7 ± 0.5). PBAT: polybutylene adipate co-terephthalate; PS-COOH: carboxylate-modified polystyrene; LSZ: lysozyme; BSA: bovine serum albumin.

from 45 to 98% (Table S1). The PS-COOH nanospheres were also mobile when no protein or BSA was present (M_{eff} = 80–99%); however, they became immobile in the presence of LSZ (M_{eff} = 0%). There was no difference in the ζ-potentials of the particles between in- and outflow, suggesting that the protein-corona was stable over the duration of the experiments.

3.2.2 Higher mobility under higher water saturation

The higher water saturation promoted the transport of pristine PBAT, weathered PBAT, and PS-COOH nanoplastics in the absence and the presence of proteins, except for PS-COOH nanospheres with LSZ, which were completely immobile (Figure 3 and Table S1). Higher water saturation of porous media enables more and bigger accessible pore spaces, thus reducing the probability of nanoplastics to interact with and attach onto solid-water interfaces[38,39]. In addition, higher water saturation corresponds to less amount of air phase in porous media, limiting the attachment of nanoplastics onto air-water interfaces as well as reducing any physical retention related to air-water interfaces or solid-water-air lines, such as pore straining, film straining, and wedging[40,41]. Further, the higher water saturation in our experiments also led to a higher pore water velocity (Table S1), and thus less time for nanoplastics to interact with either the sand-water interfaces or the air-water interfaces[21,42].

Under the higher water saturation, the pristine PBAT, weathered PBAT, and PS-COOH nanoplastics had a recovery of near 100% in the effluents in the absence of proteins (93–98%, Table S1). This indicates that physical retention of nanoplastics did not occur profoundly under the higher water saturation when there was no protein, which is expected given that the particle to collector size ratio is around 0.0007, far smaller than the threshold ratio for pore straining (0.0017) and wedging (0.005)[43–45]. In addition, the near 100% recovery suggests that nanoplastics did not attach onto the sand-water interface nor the air-water interface[22]. Indeed, the classical DLVO calculation revealed a repulsive interaction energy for the three types of nanoplastics interacting with the sand-water interface and the air-water interface (Figure S8A,B).

In comparison to the near 100% recovery under the higher water saturation, nanoplastics had a less recovery under the lower saturation in the absence of proteins (78–88%, Table S1). Because it was unfavorable for nanoplastics to attach onto the sand-water and the air-water interfaces, we attributed the less recovery of nanoplastics to physical retention processes, e.g., film straining and retention at the sand-water-air triple line, which become more important as water saturation decreases[38,46].

3.2.3 Inhibited transport of nanoplastics in the presence of LSZ

The presence of positively charged LSZ inhibited the transport of pristine PBAT and weathered PBAT nanoplastics, as indicated by the lower peak concentrations of the breakthrough curves and the lower recovery (Figure 3B,E and Table S1). For PS-COOH nanospheres, the presence of LSZ even led to the complete retention under low and high water saturations (Figure 3F). Similarly, it was reported that LSZ inhibited the transport of TiO_2 nanoparticles[47] and polystyrene nanospheres[19] in saturated porous media. Several mechanisms can be responsible for the inhibited transport of nanoplastics in the presence of LSZ, and we discuss these mechanisms in the following paragraphs.

First, the positively charged LSZ neutralized the surface charge of the negatively charged pristine PBAT, weathered PBAT, and

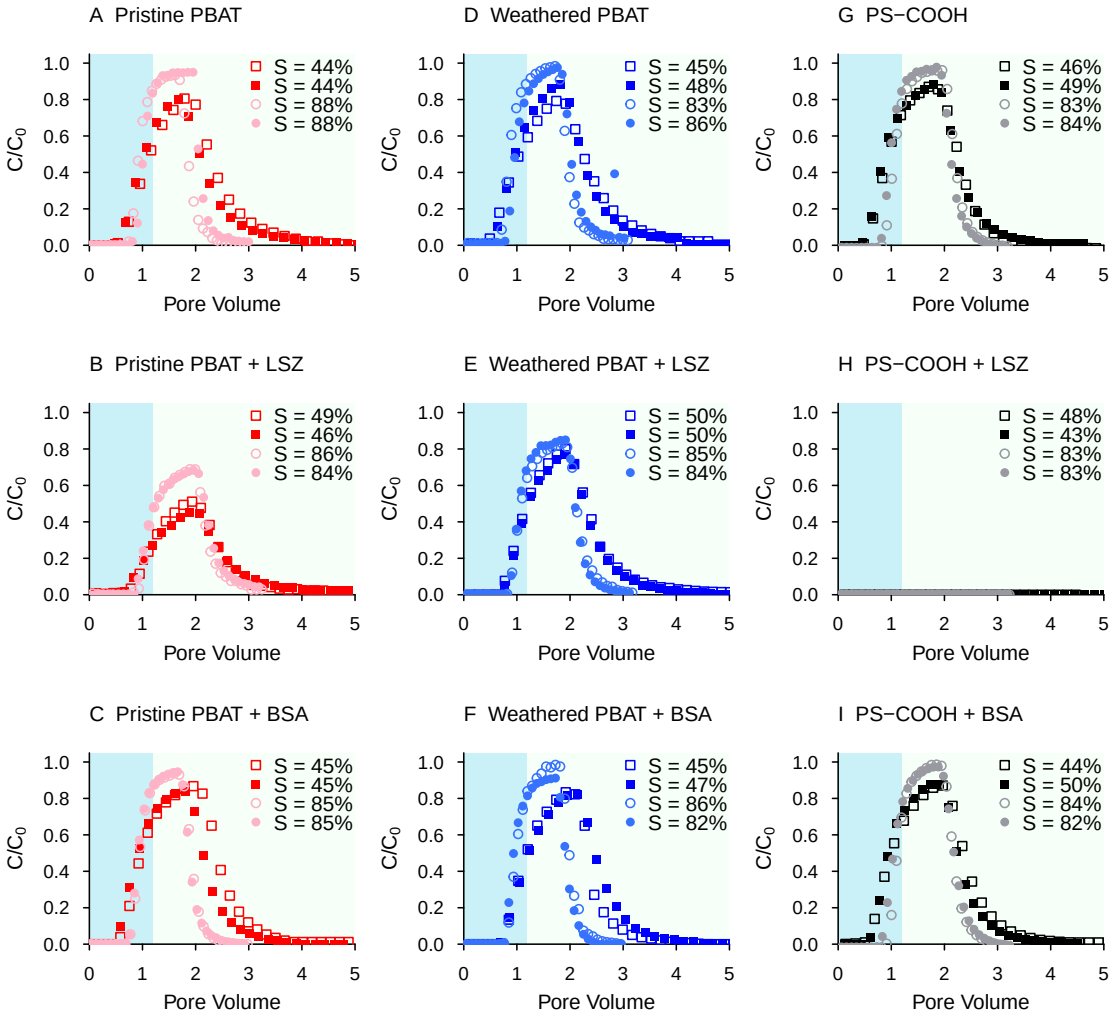

Fig. 3 Breakthrough curves of nanoplastics under unsaturated flow conditions. (A–C) Pristine PBAT nanoplastics in the absence or presence of LSZ or BSA (10 mg L^{-1}); (D–F) weathered PBAT nanoplastics in the absence or presence of LSZ or BSA (10 mg L^{-1}); (G–I) PS-COOH nanoplastics in the absence or presence of LSZ or BSA (10 mg L^{-1}). S: effective water saturation; C: nanoplastic concentration in the outflow; C_0: initial nanoplastic concentration in the inflow; pore volume = outflow volume/($\theta_v \times$ column volume). Blue and green shadings indicate the injection and elution phases of nanoplastics, respectively. PBAT: polybutylene adipate co-terephthalate; LSZ: lysozyme; BSA: bovine serum albumin; PS-COOH: carboxylate-modified polystyrene.

PS-COOH nanoplastics (Figure 1B), which would reduce the repulsive force for nanoplastics to attach onto the sand-water interface as well as the air-water interface. As expected, the energy barriers were considerably reduced on the sand-water interface for the pristine PBAT, weathered PBAT, and PS-COOH nanoplastics in the presence of LSZ (Figure S8C). However, for the air-water interface, the DLVO calculation only predicted a small energy barrier for PS-COOH nanoplastics, but an infinite energy barrier for the pristine and weathered PBAT nanoplastics (Figure S8D). This suggests that the pristine and weathered PBAT nanoplastics were unlikely to attach onto the air-water interface.

To further verify whether LSZ could promote the attachment of PBAT nanoplastics onto the air-water interface, we did subsequent wetting after the steady-state transport experiments for the pristine and weathered PBAT nanoplastics at the low water saturation (experimental details are given in Section S3, Supporting Information). We hypothesized that the subsequent wetting would remobilize any nanoplastics attached on the air-water interface. However, neither the pristine nor the weathered nanoplastics were remobilized during the subsequent wetting (Figure 4), corroborating the DLVO calculation that the pristine and weathered PBAT nanoplastics did not attach onto the air-water interface.

Compared to the pristine and weathered PBAT nanoplastics, the PS-COOH nanospheres were predicted by the classical DLVO theory to attach more readily onto the sand-water and the air-water interface in the presence of LSZ (Figure S8C,D). This is expected, because in the presence of LSZ, the PS-COOH nanospheres became positively charged and even aggregated. Other than the more favorable attachment, physical straining would also occur for the PS-COOH nanospheres due to their large aggregate size; however, physical straining is unlikely to occur

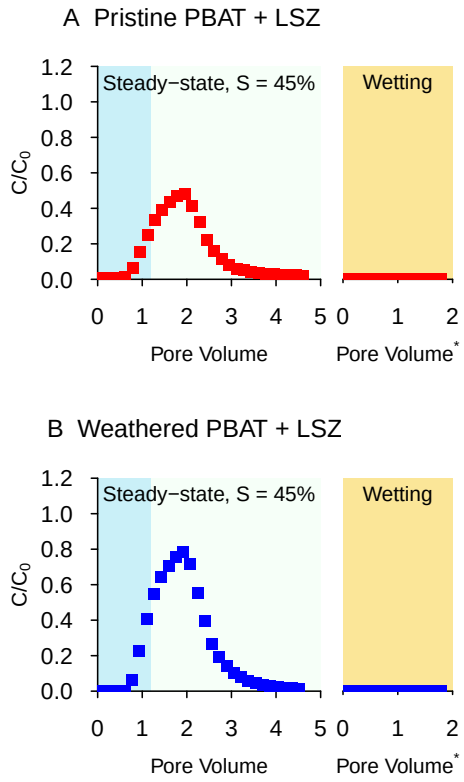

Fig. 4 Breakthrough curves of nanoplastics during steady-state flow and wetting. (A) Pristine PBAT nanoplastics in the presence of LSZ (10 mg L^{-1}); (B) weathered PBAT nanoplastics in the presence of LSZ (10 mg L^{-1}). S: effective water saturation; C: nanoplastic concentration in the outflow; C_0: initial nanoplastic concentration in the inflow; pore volume = outflow volume/($\theta_v \times$ column volume); pore volume*: θ_v is set to the porosity for the wetting phase. The blue and green shadings indicate the injection and elution phases of nanoplastics during the steady-state, respectively, and the yellow shading indicates the wetting phase. PBAT: polybutylene adipate co-terephthalate; LSZ: lysozyme.

for the pristine and weathered PBAT nanoplastics, which did not aggregate in the presence of LSZ. The hydrodynamic diameter of the PS-COOH nanospheres was 857 nm at the beginning of the transport experiments (Figure 1C), resulting in a particle-collector ratio of 0.0025 that exceeds the threshold for pore straining (particle-collector ratio of 0.0017) under saturated conditions[43]. Similarly, Dong et al.[19] also attributed the enhanced retention of 200 nm polystyrene nanospheres in the presence of LSZ to decreased repulsive interaction and straining.

3.2.4 Transport of nanoplastics not affected by BSA

In contrast to the positively charged LSZ, the negatively charged BSA did not inhibit nor enhance the transport of the pristine PBAT, weathered PBAT, and PS-COOH nanoplastics (Figure 3 and Table S1). It is expected that BSA would not inhibit the transport of nanoplastics, given that BSA could not promote aggregation and thus also not physical straining of nanoplastics, nor could it significantly reduce the electrostatic repulsion and therefore the attachment of nanoplastics onto the sand-water interface or the air-water interface (Figure S8E,F). In fact, BSA has been reported previously to enhance the transport of colloidal particles (e.g., biochar colloids, kaolinite colloids, and nanoplastics), because BSA forms protein-coronas around colloidal particles and thereby exerts steric repulsion that prevents colloidal particles from attaching onto the sand-water interface or the air-water interface[19,48,49]. Although our results show that BSA formed protein-coronas around nanoplastics, the presence of BSA did not further enhance the transport of nanoplastics, indicating that BSA-induced steric interaction did not contribute to the mobility of nanoplastics. Thus, as in the case without proteins, in the presence of BSA, the pristine PBAT, weathered PBAT, and PS-COOH nanoplastics could only be retained via physical straining in the unsaturated sand column under the lower water saturation.

3.2.5 Comparison of mobility between PBAT and PS-COOH nanoplastics

In the absence of proteins or in the presence of BSA, the pristine and weathered PBAT nanoplastics showed similar mobility as the PS-COOH nanoplastics under the two water saturations (Figure 3A,C,D,F,G,I and Table S1). The similar mobility is, on the one hand, due to the similar sizes of the three types of nanoplastics, a size too small to be affected by physical straining (Figure 1C). On the other hand, despite their differences in surface charges, the pristine PBAT, weathered PBAT, and PS-COOH nanoplastics all experienced sufficient repulsion that prevented the attachment onto the sand-water interface and the air-water interface (Figure S8A,B,E,F).

Additionally, the pristine and weathered PBAT nanoplastics had similar mobility in the absence of proteins, suggesting that UV-weathering did not promote the transport of PBAT nanoplastics. This, however, is inconsistent with previous studies where UV-weathering has been found to enhance the transport of micro- and nanoplastics (e.g., polylactic acid, polyvinyl chloride, and polystyrene) via introducing O-containing functional groups[50,51]. In our study, we indeed found that the weathered PBAT contained more O-functional groups than the pristine PBAT (Figure 1A), but the weathered PBAT did not have higher mobility. This can be attributed to the high mobility of the pristine PBAT nanoplastics themselves, which outweighed the contribution of UV-weathering.

In the presence of LSZ, the pristine and weathered PBAT nanoplastics had profoundly higher mobility than the PS-COOH nanoplastics (Figure 3B,E,H). This difference can be attributed to the distinct ways in which the three types of nanoplastics interacted with LSZ. As discussed before, LSZ induced surface charge reversal and aggregation of the PS-COOH nanoplastics, thus led to the complete retention of the PS-COOH nanoplastics; while LSZ only increased surface charges of the pristine and weathered PBAT nanoplastics, resulting in enhanced retention. However, compared to the weathered PBAT nanoplastics, the pristine PBAT nanoplastics were retained more in the presence of LSZ, despite that the surface charge of the pristine PBAT nanoplastics was less affected by LSZ. This is likely due to less interaction between LSZ and the pristine PBAT nanoplastics that freed more LSZ to attach onto the sand-water interfaces, providing additional attachment sites for the pristine PBAT nanoplastics. To test this hypothesis,

we first flushed the sand column with LSZ and then injected the pristine PBAT nanoplastics into the column (experimental details are given in Section S4, Supporting Information). Indeed, we found that LSZ was completely retained in the sand column (Figure S10A) and the transport of the pristine PBAT nanoplastics was inhibited in the sand column in which LSZ were completely retained (Figure S10B).

4 Conclusions

Biodegradable plastics have attracted a lot of attention due to their promising potential to replace conventional plastics for many products, particularly single-use items, such as plastic cutlery, shopping bags, and plastic mulch films. However, recent studies have shown that soil-biodegradable plastics generate more abundant micro- and nanoplastics than conventional plastics during biodegradation in the environment, and concern has been raised about the environmental impacts of these soil-biodegradable micro- and nanoplastics. These soil-biodegradable micro- and nanoplastics will reside in soils only temporarily as they continue to biodegrade into CO_2, H_2O, and microbial biomass; but nonetheless, they may negatively impact soil and environmental health before they completely degrade. It is also possible that these soil-biodegradable micro- and nanoplastics move off from their intended end-of-life location, i.e., the topsoil, where biodegradation is highest, and translocate to locations where biodegradation is less favorable.

Here, we show that soil-biodegradable nanoplastics made of PBAT are highly mobile in sandy porous media; but when plastics are exposed to environmental conditions, eco-corona formation will change surface properties and transport behavior. Negatively charged proteins will not affect the transport behavior of the nanoplastics; however, the coverage of positively charged protein-coronas can change the surface charge of the nanoplastics, and thereby render nanoplastics less mobile. In addition, our study shows that decreasing water saturation hinders the transport of soil-biodegradable nanoplastics, and thus unsaturated soils will be more prone to retain the nanoplastics in the topsoil, where microbial activity is the highest and biodegradation of the plastic particles will be most prevalent. Future research is still needed to advance our understanding about the fate and transport of soil-biodegradable plastics in the environment, and to ensure informative adoption and sustainable use of soil-biodegradable plastic products.

Author Contributions

YY and MF conceived and designed the research; YY and MF led overall study; YY and MF wrote manuscript and analyzed data; OQ, LK, YY and MF performed transmission electron microscopy; AA and DG provided soil-biodegradable plastic materials and performed FTIR analysis; all co-authors contributed to data interpretation and editing.

Conflicts of interest

There are no conflicts to declare.

Acknowledgements

This work was supported by NSF Grant 2152514 from the NSF-EAR Geobiology and Low-Temperature Geochemistry program and W4188 Multi-State Hatch Project. A portion of this research was performed on a project award https://doi.org/10.46936/expl.proj.2020.51632/60000231 from the Environmental Molecular Sciences Laboratory, a DOE Office of Science User Facility sponsored by the Biological and Environmental Research program under Contract No. DE-AC05-76RL01830.

Notes and references

1 A. A. Horton, A. Walton, D. J. Spurgeon, E. Lahive and C. Svendsen, Microplastics in freshwater and terrestrial environments: Evaluating the current understanding to identify the knowledge gaps and future research priorities, *Sci. Total Environ.*, 2017, **586**, 127–141.

2 M. Bläsing and W. Amelung, Plastics in soil: Analytical methods and possible sources, *Sci. Total Environ.*, 2018, **612**, 422–435.

3 F. Corradini, P. Meza, R. Eguiluz, F. C. E. Huerta-Lwanga and V. Geissen, Evidence of microplastic accumulation in agricultural soils from sewage sludge disposal, *Sci. Total Environ.*, 2019, **671**, 411–420.

4 A. A. de Souza Machado, C. W. Lau, J. Till, W. Kloas, A. Lehmann, R. Becker and M. C. Rillig, Impacts of microplastics on the soil biophysical environment, *Environ. Sci. Technol.*, 2018, **52**, 9656–9665.

5 L. Li, Y. Luo, R. Li, Q. Zhou, W. J. Peijnenburg, N. Yin, J. Yang, C. Tu and Y. Zhang, Effective uptake of submicrometre plastics by crop plants via a crack-entry mode, *Nat. Sustain.*, 2020, **3**, doi:10.1038/s41893–020–0567–9.

6 H. Y. Sintim and M. Flury, Is Biodegradable Plastic Mulch the Solution to Agriculture's Plastic Problem?, *Environ. Sci. Technol.*, 2017, **51**, 1068–1069.

7 T. S. Galloway, M. Cole and C. Lewis, Interactions of microplastic debris throughout the marine ecosystem, *Nat. Ecol. Evol.*, 2017, **1**, 0116, doi:10.1038/s41559–017–0116.

8 Y. Yu, D. E. Griffin-LaHue, C. A. Miles, D. G. Hayes and M. Flury, Are Microplastics from Biodegradable Plastic Mulches an Environmental Concern?, *J. Hazard. Mater. Advances*, 2021, **4**, 100024, doi:10.1016/j.hazadv.2021.100024.

9 M. Sander, Biodegradation of polymeric mulch films in agricultural soils: concepts, knowledge gaps, and future research directions, *Environ. Sci. Technol.*, 2019, **53**, 2304–2315.

10 M. Flury and R. Narayan, Biodegradable Plastic as Integral Part of the Solution to Plastic Waste Pollution of the Environment, *Curr. Opin. Green Sustain. Chem.*, 2021, **30**, 100490, doi:10.1016/j.cogsc.2021.100490.

11 H. Y. Sintim, A. I. Bary, D. G. Hayes, L. C. Wadsworth, M. B. Anunciado, M. E. English, S. Bandopadhyay, S. M. Schaeffer, J. M. DeBruyn, C. A. Miles, J. P. Reganold and M. Flury, In situ degradation of biodegradable plastic mulch films in compost and agricultural soils, *Sci. Total Environ.*, 2020, **727**, 138668,

doi:10.1016/j.scitotenv.2020.138668.

12 D. E. Griffin-LaHue, S. Ghimire, Y. Yu, E. J. Scheenstra, C. A. Miles and M. Flury, In-Field Degradation of Soil-Biodegradable Plastic Mulch Films in a Mediterranean Climate, *Sci. Total Environ.*, 2022, **806**, 150238, doi:10.1016/j.scitotenv.2021.150238.

13 Y. Yu, M. Velandia, D. G. Hayes, L. W. DeVetter, C. A. Miles and M. Flury, Biodegradable plastics as alternatives for polyethylene mulch films, *Adv. Agron.*, 2024, **183**, 121–192, doi:10.1016/bs.agron.2023.10.003.

14 L. Schöpfer, R. Menzel, U. Schnepf, L. Ruess, S. Marhan, F. Brümmer, H. Pagel and E. Kandeler, Microplastics effects on reproduction and body length of the soil-dwelling nematode *Caenorhabditis elegans*, *Front. Environ. Sci.*, 2020, **8**, 41, doi:10.3389/fenvs.2020.00041.

15 Y. Qi, N. Beriot, G. Gort, E. H. Lwanga, H. Gooren, X. Yang and V. Geissen, Impact of plastic mulch film debris on soil physicochemical and hydrological properties, *Environ. Pollut.*, 2020, **266**, 115097, doi:10.1016/j.envpol.2020.115097.

16 Y. Liu, Y. Hu, C. Yang, C. Chen, W. Huang and Z. Dang, Aggregation kinetics of UV irradiated nanoplastics in aquatic environments, *Water Res.*, 2019, **163**, 114870, doi:10.1016/j.watres.2019.114870.

17 X. Li, E. He, B. Xia, Y. Liu, P. Zhang, X. Cao, L. Zhao, X. Xu and H. Qiu, Protein corona-induced aggregation of differently sized nanoplastics: impacts of protein type and concentration, *Environ. Sci. Nano*, 2021, **8**, 1560–1570.

18 Y. Yu, A. F. Astner, T. M. Zahid, I. Chowdhury, D. G. Hayes and M. Flury, Aggregation kinetics and stability of biodegradable nanoplastics in aquatic environments: Effects of UV-weathering and proteins, *Water Res.*, 2023, **239**, 120018, doi:10.1016/j.watres.2023.120018.

19 Z. Dong, Y. Hou, W. Han, M. Liu, J. Wang and Y. Qiu, Protein corona-mediated transport of nanoplastics in seawater-saturated porous media, *Water Res.*, 2020, **182**, 115978, doi:10.1016/j.watres.2020.115978.

20 J. Shang, M. Flury, J. B. Harsh and R. L. Zollars, Comparison of Different Methods to Measure Contact Angles of Soil Colloids, *J. Colloid Interface Sci.*, 2008, **328**, 299–307.

21 Y. Yu, M. Elliott, I. Chowdhury and M. Flury, Transport Mechanisms of Motile and Non-motile *Phytophthora cactorum* Zoospores in Unsaturated Porous Media, *Water Resour. Res.*, 2021, **57**, e2020WR028249, doi:10.1029/2020WR028249.

22 Y. Yu, H. Y. Sintim, A. F. Astner, D. G. Hayes, A. Bary, A. Zelenyuk, O. Qafoku, L. Kovarik and M. Flury, Enhanced Transport of TiO_2 in Unsaturated Sand and Soil after Release from Biodegradable Plastic during Composting, *Environ. Sci. Technol.*, 2022, **56**, 2398–2406, doi:10.1021/acs.est.1c07169.

23 J. Šimunek, M. Šejna and M. T. Van Genuchten, *The HYDRUS-1D software package for simulating the one-dimensional movement of water, heat, and multiple solutes in variably-saturated media, Version 2.0*, IGWMC-TPS, Golden, CO, 1998.

24 D. G. Hayes, L. C. Wadsworth, H. Y. Sintim, M. Flury, M. English, S. Schaeffer and A. M. Saxton, Effect of diverse weathering conditions on the physicochemical properties of biodegradable plastic mulches, *Polym. Test*, 2017, **62**, 454–467.

25 R. Qiao, C. Zhao, J. Liu, M. Zhang and W. He, Synthesis of Novel Ultraviolet Absorbers and Preparation and Field Application of Anti-Ultraviolet Aging PBAT/UVA Films, *Polymers*, 2022, **14**, 1434, doi:10.3390/polym14071434.

26 Z. Wang, J. Ding, X. Song, L. Zheng, J. Huang, H. Zou and Z. Wang, Aging of poly (lactic acid)/poly (butylene adipate-co-terephthalate) blends under different conditions: Environmental concerns on biodegradable plastic, *Sci. Total Environ.*, 2023, **855**, 158921, doi:10.1016/j.scitotenv.2022.158921.

27 S. Badaire, C. Cottin-Bizonne and A. D. Stroock, Experimental investigation of selective colloidal interactions controlled by shape, surface roughness, and steric layers, *Langmuir*, 2008, **24**, 11451–11463.

28 M. Elimelech, J. Gregory and X. Jia, *Particle deposition and aggregation: measurement, modelling and simulation*, Butterworth-Heinemann, Woburn, MA, 2013.

29 Y. Lan, A. Caciagli, G. Guidetti, Z. Yu, J. Liu, V. E. Johansen, M. Kamp, C. Abell, S. Vignolini, O. A. Scherman *et al.*, Unexpected stability of aqueous dispersions of raspberry-like colloids, *Nat. Commun.*, 2018, **9**, 1–8, doi:10.1038/s41467–018–05560–3.

30 X. Li, E. He, K. Jiang, W. J. Peijnenburg and H. Qiu, The crucial role of a protein corona in determining the aggregation kinetics and colloidal stability of polystyrene nanoplastics, *Water Res.*, 2021, **190**, 116742, doi:10.1016/j.watres.2020.116742.

31 K. Hagiya, A. Miyagawa, S. Nagatomo and K. Nakatani, Direct Quantification of Proteins Modified on a Polystyrene Microparticle Surface Based on ζ Potential Change, *Anal. Chem.*, 2022, **94**, 6304–6310.

32 C. Vasti, D. A. Bedoya, R. Rojas and C. E. Giacomelli, Effect of the protein corona on the colloidal stability and reactivity of LDH-based nanocarriers, *J. Mater. Chem. B*, 2016, **4**, 2008–2016.

33 J. Piella, N. G. Bastús and V. Puntes, Size-dependent protein–nanoparticle interactions in citrate-stabilized gold nanoparticles: the emergence of the protein corona, *Bioconjug. Chem.*, 2017, **28**, 88–97.

34 C. Yan, T. Cheng, B. Li and J. Shang, Distinct interactions of pig and cow manure-derived colloids with TiO_2 nanoparticles and their impact on stability and transport, *J. Hazard. Mater.*, 2021, **416**, 125910, doi:10.1016/j.jhazmat.2021.125910.

35 D. Schweich and M. Sardin, Adsorption, partition, ion exchange and chemical reaction in batch reactors or in columns—A review, *J. Hydrol.*, 1981, **50**, 1–33.

36 A. A. Keller, S. Sirivithayapakorn and C. V. Chrysikopoulos, Early breakthrough of colloids and bacteriophage MS2 in a water-saturated sand column, *Water Resour. Res.*, 2004, **40**, W08304, doi:10.1029/2003WR002676.

37 Z. You, A. Badalyan, P. Bedrikovetsky *et al.*, Size-exclusion colloidal transport in porous media-stochastic modeling and experimental study, *SPE Journal*, 2013, **18**, 620–633.

38 T. Knappenberger, M. Flury, E. D. Mattson and J. B. Harsh, Does water content or flow rate control colloid transport in unsaturated porous media?, *Environ. Sci. Technol.*, 2014, **48**, 3791–3799.

39 T. Knappenberger, S. Aramrak and M. Flury, Transport of barrel and spherical shaped colloids in unsaturated porous media, *J. Contam. Hydrol.*, 2015, **180**, 69–79.

40 S. Torkzaban, S. A. Bradford, M. T. van Genuchten and S. L. Walker, Colloid transport in unsaturated porous media: The role of water content and ionic strength on particle straining, *J. Contam. Hydrol.*, 2008, **96**, 113–127.

41 Y. Yu and M. Flury, Current understanding of subsurface transport of micro- and nanoplastics in soil, *Vadose Zone J.*, 2021, **20**, e20108, doi:10.1002/vzj2.20108.

42 S. Rahmatpour, M. R. Mosaddeghi, M. Shirvani and J. Simunek, Transport of silver nanoparticles in intact columns of calcareous soils: the role of flow conditions and soil texture, *Geoderma*, 2018, **322**, 89–100.

43 S. A. Bradford, S. R. Yates, M. Bettahar and J. Simunek, Physical factors affecting the transport and fate of colloids in saturated porous media, *Water Resour. Res.*, 2002, **38**, 1327, doi:10.1029/2002WR001340.

44 S. A. Bradford, J. Šimunek, M. Bettahar, M. T. Van Genuchten and S. R. Yates, Significance of straining in colloid deposition: Evidence and implication, *Water Resour. Res.*, 2006, **42**, 12–15.

45 W. Johnson, X. Li and G. Yal, Colloid retention in porous media: Mechanistic confirmation of wedging and retention in zones of flow stagnation, *Environ. Sci. Technol.*, 2007, **41**, 1279–1287.

46 M. Flury and S. Aramrak, Role of Air-Water Interfaces in Colloid Transport in Porous Media: A Review, *Water Resour. Res.*, 2017, **53**, 5247–5275.

47 J. Rottman, L. C. Platt, R. Sierra-Alvarez and F. Shadman, Removal of TiO_2 nanoparticles by porous media: effect of filtration media and water chemistry, *Chem. Eng. J.*, 2013, **217**, 212–220.

48 C. Yan, T. Cheng and J. Shang, Effect of bovine serum albumin on stability and transport of kaolinite colloid, *Water Res.*, 2019, **155**, 204–213.

49 W. Yang, S. A. Bradford, Y. Wang, P. Sharma, J. Shang and B. Li, Transport of biochar colloids in saturated porous media in the presence of humic substances or proteins, *Environ. Pollut.*, 2019, **246**, 855–863.

50 J. Liu, T. Zhang, L. Tian, X. Liu, Z. Qi, Y. Ma, R. Ji and W. Chen, Aging significantly affects mobility and contaminant-mobilizing ability of nanoplastics in saturated loamy sand, *Environ. Sci. Technol.*, 2019, **53**, 5805–5815.

51 J. Fei, H. Xie, Y. Zhao, X. Zhou, H. Sun, N. Wang, J. Wang and X. Yin, Transport of degradable/nondegradable and aged microplastics in porous media: Effects of physicochemical factors, *Sci. Total Environ.*, 2022, **851**, 158099, doi:10.1016/j.scitotenv.2022.158099.